THE JOURNAL OF PHYSICAL CHEMISTRY B

ARTICLE

pubs.acs.org/JPCB

pH-Dependent Reactivity for Glycyl-L-tyrosine in Carboxypeptidase-A-Catalyzed Hydrolysis

Shanshan Wu,[†,⊥] Chunchun Zhang,[‡,⊥] Ruyin Cao,[†] Dingguo Xu,[*,†] and Hua Guo[§]

[†]College of Chemistry, MOE Key Laboratory of Green Chemistry and [‡]Analytical&Testing Center, Sichuan University, Chengdu, Sichuan 610064, People's Republic of China

[§]Department of Chemistry and Chemical Biology, University of New Mexico, Albuquerque, New Mexico 87131, United States

Supporting Information

ABSTRACT: The dipeptide glycyl-L-tyrosine (GY) can be either a substrate for carboxypeptidase A (CPA) or an inhibitor, depending on pH. In this work, we investigate the pH-dependent reactivity of this dipeptide in CPA-catalyzed hydrolysis using a combined quantum mechanical and molecular mechanical method. It is shown that the monoionic form of the dipeptide, prevalent at high pH, chelates the active site zinc ion, rendering the enzyme inactive. This inhibitory form is consistent with an earlier X-ray structure of the CPA−GY complex. On the other hand, the prevailing di-ionic form of the dipeptide at low pH was found to undergo hydrolysis via a nucleophilic mechanism, leading to an acyl−enzyme complex. The stability of this reaction intermediate is consistent with previous low-temperature solid-state NMR results. The calculated overall free-energy barrier of 20.1 kcal/mol is in excellent agreement with the experimental value of 19.9 kcal/mol.

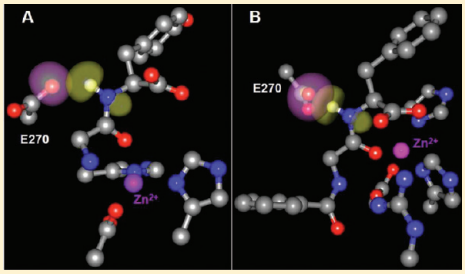

1. INTRODUCTION

Carboxypeptidase A (CPA, EC 3.4.17.1) is a zinc-containing protease secreted by the pancreas. It catalyzes the hydrolytic removal of a C-terminal amino acid with a preference for a hydrophobic side chain.[1] It occupies a special place in enzymology as the third enzyme whose three-dimensional structure was determined with high resolution by X-ray diffraction.[2] Thanks to the availability of its structure, CPA has also played an important role in the early development of therapeutic agents for many clinically important zinc peptidases, such as the blood pressure regulating angiotensin converting enzyme (ACE).[3,4] As a result, there have been many structural and kinetic studies on CPA.[5]

The numerous three-dimensional structures of apo CPA and its complexes with various ligands revealed that the zinc ion is coordinated by three active site residues His69, Glu72, and His196, and its fourth ligand in its ligand-free state is a water molecule.[6−21] Despite the abundance of structural information, however, there were still controversies concerning its catalytic mechanism.[5] As depicted in Figure 1, two major reaction mechanisms have been proposed. The so-called promoted water pathway,[22−25] which is essentially the general base/general acid mechanism, envisages the zinc-bound water as the nucleophile, which attacks the scissile carbonyl carbon with the assistance of an active site general base, namely, Glu270. In the elimination step, the protonated Glu270 acts as the general acid to protonate the amide nitrogen leaving group. The alternative mechanism of the nucleophilic or "anhydride" pathway[26−30] features the direct nucleophilic addition of the carboxylate side chain of Glu270 to the scissile carbonyl carbon, forming an acyl−enzyme (AE) complex, which is eventually hydrolyzed by water. Evidence for both mechanistic proposals has been reviewed by Christianson and Lipscomb.[5]

Recently, we have analyzed the mechanisms for CPA-catalyzed hydrolysis of both peptide and ester substrates using a reliable quantum mechanical/molecular mechanical (QM/MM) method.[31,32] It was shown that the promoted water pathway is viable for both types of substrates. On the other hand, the nucleophilic pathway is blocked for the hydrolysis of peptide but partially viable for ester substrates. Indeed, an AE complex was found to be stable in the nucleophilic pathway, but the high barrier associated with its further hydrolysis renders it noncompetitive with the promoted water pathway at room temperature. These, and other theoretical results,[33−37] helped us to understand the existing experimental evidence concerning CPA catalysis.

However, the CPA-catalyzed hydrolysis of dipeptides seems to deviate significantly from the canonical mechanism discussed above.[38,39] Taking the example of glycyl-L-tyrosine (GY), it has an unusually slow k_{cat} (0.9 min^{-1}) for hydrolysis.[40] In addition, the high-resolution X-ray structure by Christianson and Lipscomb indicates that the substrate directly binds to the zinc ion with a chelating configuration,[13] in which the carbonyl oxygen and the N-terminal amino nitrogen bind the zinc ion simultaneously. Such a binding pattern excludes the possibility of an active site water near the zinc ion and thus promotes water pathway. On the other hand, a low-temperature solid-state NMR study by Lee et al.[41] in 1998 detected the signal of the anhydride

Received: May 18, 2011
Revised: July 1, 2011
Published: July 06, 2011

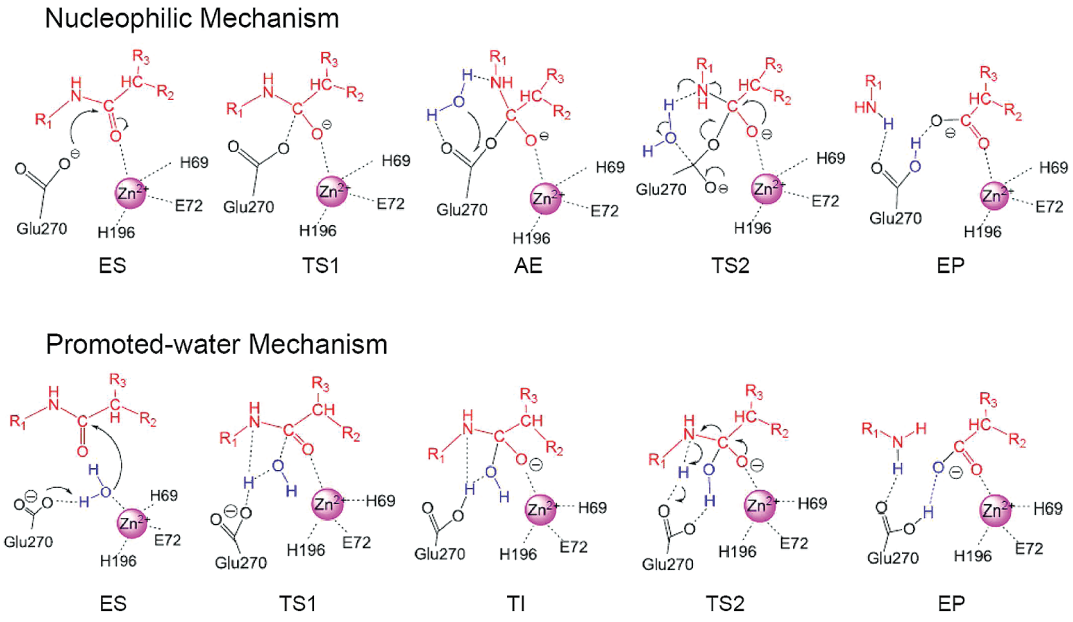

Figure 1. Two putative mechanisms for the hydrolysis of peptides catalyzed by CPA.

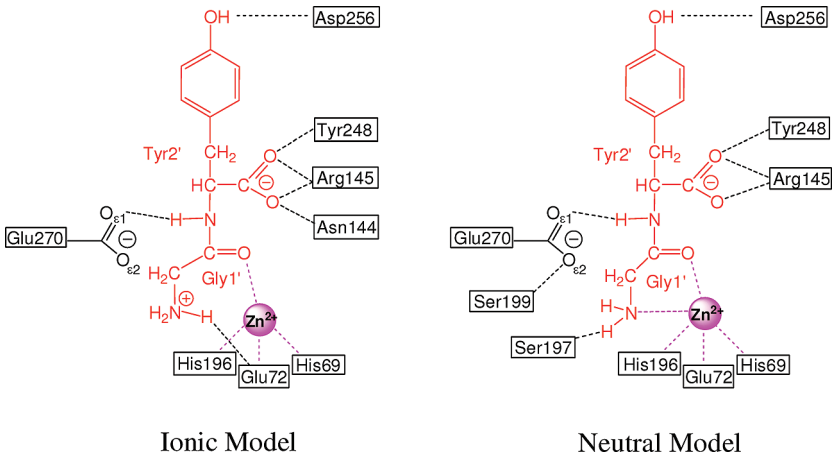

Figure 2. Atom definitions for the ES_{ionic} (left) and $ES_{neutral}$ (right) models.

intermediate in the CPA-catalyzed hydrolysis of GY, which might be construed as the direct evidence in support of the nucleophilic pathway.

To reconcile these differences, it is important to note that the N-terminal of a dipeptide is in the active site of CPA, while that for an oligopeptide is generally far away from the catalytic zinc ion. In addition, this amino nitrogen of the dipeptide ligand may have different protonation states, which might in turn alter the reactivity of the ligand. Indeed, the earlier work of Yanari and Mitz suggested that GY is a substrate (albeit a slow one) at low pH, but it turns into an inhibitor at high pH.[39] This is consistent with the X-ray structure of the CPA−GY complex (which was prepared with pH > 7),[5] in which the N-terminal amino nitrogen of the peptide is obviously neutral, judging from its coordination with the zinc ion. This observation is an intriguing one, and it can be used to design useful inhibitors. Indeed, Lee et al. have carried out a series of inhibitor design studies based on the binding pattern of GY.[42] However, the mechanism for the pH-dependent reactivity in CPA catalysis of GY hydrolysis remains to be elucidated.

In this work, we report a computational study to address the hydrolysis mechanism of GY catalyzed by CPA and its pH dependence. This article is organized as follows; the next section will provide the setup protocol and computational details. This is followed by the results and discussion section. A summary is presented in the final section.

2. METHOD

2.1. QM/MM Models. The hybrid QM/MM approach[43] has been proven to be a reliable and efficient way to simulate extended systems such as enzymes.[44−46] Its principles have been discussed extensively in the literature;[47] therefore, we only give a brief description here. In the QM/MM framework, the system is divided into two parts; the smaller reactive region is treated with a QM method, while the rest of system is described by a MM

dx.doi.org/10.1021/jp2046504 |J. Phys. Chem. B 2011, 115, 10360–10367

approach. As in our previous work on CPA,[31,32] we employed here the SCC-DFTB/CHARMM approach, in which the QM region is treated at the self-consistent charge density functional tight binding (SCC-DFTB) model[48] while the MM region is treated with the CHARMM force field.[49] SCC-DFTB is an approximate density functional method[50] with parametrization for biological zinc ions.[51] It has been demonstrated to give a reasonably accurate description of active sites of several zinc enzymes and their catalysis.[52−57]

To understand the influence of pH on binding and catalysis of CPA, we constructed two models for the GY ligand with different protonation states in its N-terminal amino group. The first neutral model is based on the X-ray structure of CPA complexed with GY (PDB code 3CPA),[13] in which the chelating pattern of the GY in the CPA active site strongly suggests that the GY ligand has a neutral N-terminal amino group. This enzyme−substrate complex is thus denoted as the $ES_{neutral}$. Its counterpart in the second ionic model, labeled as ES_{ionic}, adopts a positive charged N-terminal ammonium group for GY to simulate the acidic environment as suggested in the ref 39. The protonation states of all titratable residues in ES_{ionic} were chosen to be the same as those in $ES_{neutral}$. There are some uncertainties in the structure of the former as no X-ray structure exists. However, we believe that the changes of protonation states at lower pH will mostly occur on the surface of CPA, which will be effectively screened by the solvent.

The setup protocol is similar to our recent work on CPA.[31,32] Both models were solvated using a pre-equilibrated TIP3P water[58] sphere with a 25 Å radius centered at the zinc ion. This procedure was repeated several times with rotated water spheres to ensure uniform solvation. The solvent was relaxed with a 30 ps molecular dynamics (MD) run with all protein and substrate atoms fixed. Stochastic boundary conditions[59] were applied to reduce computational costs. In particular, the system was divided into three zones and treated with different approaches. The atoms in inner reaction zone (r < 22 Å) were treated with Newtonian dynamics, while the atoms in the buffer zone (22 < r < 25 Å) were treated using Langevin dynamics. Finally, the atoms in the reservoir zone (r > 25 Å) were removed. The link atom approach[60] was applied at the boundary between the QM and MM regions. A group-based switching scheme was applied for nonbonded interactions.[61]

As depicted in Figure 2, the QM region for both models consists of the entire substrate, the zinc ion, and side-chain groups of His69, Glu72, His196, and Glu270. In the subsequent hydrolysis step of the AE intermediate, an additional water molecule was introduced into the QM region to serve as the nucleophile. It is located between the Glu270 side-chain group and the substrate molecule.

The ES complexes were then subjected to a 800 ps QM/MM MD simulation to study the active site dynamics. The systems were first heated slowly from 0 to 300 K within 30 ps, followed by 270 ps of equilibration at room temperature. The subsequent 500 ps MD trajectories were used for data analysis. For the AE complex, we also performed a 700 ps MD simulation with first 200 ps for heating and equilibration and the rest of the 500 ps for data analysis. The integration step for MD simulations was 1.0 fs, and the SHAKE algorithm[62] was applied to keep all covalent bonds involving hydrogen atoms.

To simulate the reaction process, we first extracted snapshots from the MD trajectories of the ES complexes. After minimization, minimum energy paths (MEPs) were calculated using the adiabatic mapping approach along the putative reaction coordinates. Because there is no water in the active site for the CPA−GY complex, we will focus on the nucleophilic pathway. To this end, the reaction coordinate for the first acylation (A) step was defined as $r_1 = d_{C(G1')\cdots O_{\varepsilon}(E270)}$, while that for the second deacylation (DA) is given as $r_2 = d_{H_1\cdots O_w} - d_{H_1\cdots N(Y2')}$. To confirm the accuracy of the SCC-DFTB/CHARMM method, single-point calculations were performed at the B3LYP/CHARMM level of theory along the reaction coordinates for which the structures were determined by the SCC-DFTB/CHARMM Hamiltonian. In this work, the standard 6-31G(d) basis set was used for the C, H, O, and N atoms, and the Lan12DZ ECP basis set was used for the zinc ion. These calculations were performed using a GAMESS-UK/CHARMM interface.[63] The comparison of the minimal energy profiles is given in Supporting Information (SI), which shows good agreement.

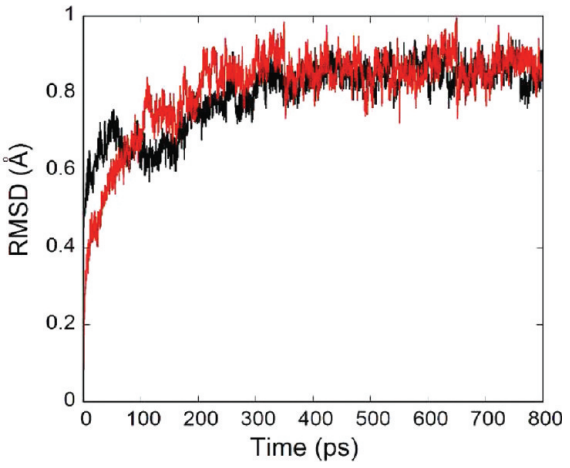

Figure 3. The rmsd for backbone fluctuations of the ES_{ionic} (black line) and $ES_{neutral}$ (red line) complexes.

In the calculation of the potentials of mean force (PMFs), the umbrella sampling method[64] was used to enhance the sampling around high-energy regions. In particular, the reaction coordinate was divided into a number of windows, and harmonic bias potentials was used to constrain the system. For the neutral model, only the A step was investigated, and 12 windows were used, each with a force constant of 150 kcal/mol·Å^2. For the ionic model, on the other hand, a total of 13 and 11 windows were used for the A and DA steps, respectively. The harmonic force constant of the bias potential ranged from 100 to 150 kcal/mol·Å^2. In each window, a total of 100 ps of constrained MD simulation was performed. The first 60 ps was for equilibration, and the rest of the 40 ps simulation was used to evaluate the distribution function along the reaction coordinate. The final PMFs were obtained using the weighted histogram analysis method (WHAM).[65]

2.2. Natural Bond Orbital Studies. To explain the different reactivities of several substrates in the reaction catalyzed by CPA, we constructed three truncated active site models, which contain all of the atoms of the QM region for CPA complexed with GY, hippuryl-L-Phe (HPL), and hippuryl-D,L-β-phenyllactate (HPL). Natural bond orbital (NBO)[66] calculations were carried out on these models using the B3LYP functional with the 6-31G* basis set.

3. RESULTS

3.1. Neutral Model. The $ES_{neutral}$ complex is quite stable throughout the 800 ps QM/MM MD simulation, evidenced by

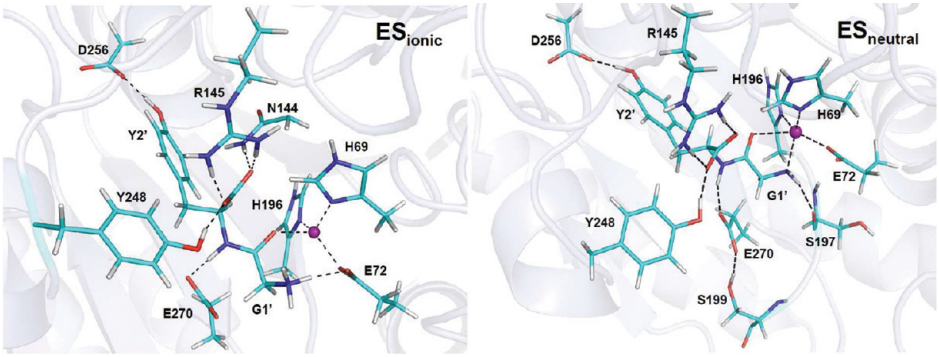

Figure 4. Snapshots from MD simulations of ES_{ionic} and $ES_{neutral}$.

Table 1. Selected Geometric Parameters for the $ES_{neutral}$ Model Obtained from the SCC-DFTB/MM MD Simulation

distance (Å)	QM/MM MD ES	expt.[13]
$Zn\cdots N_{\delta 1}(H69)$	1.99 ± 0.04	2.1
$Zn\cdots O_{\varepsilon 2}(E72)$	2.13 ± 0.03	2.3
$Zn\cdots N_{\delta 1}(H196)$	2.00 ± 0.06	2.1
$Zn\cdots O(G1')$	2.39 ± 0.18	2.3
$Zn\cdots N(G1')$	2.13 ± 0.11	1.9
$O(S197)\cdots H_{\tau 1}(G1')$	1.76 ± 0.19 (2.83 ± 0.21[a])	2.8[a]
$H_{\eta 1}(S199)\cdots O_{\varepsilon 2}(E270)$	1.66 ± 0.15 (2.69 ± 0.12[b])	2.7[b]
$C(G1')\cdots O_{\varepsilon 2}(E270)$	4.88 ± 0.29	3.6
$HN(Y2')\cdots O_{\varepsilon 1}(E270)$	2.01 ± 0.27 (2.99 ± 0.29[a])	2.6[a]
$O_{\tau 2}(Y2')\cdots H_{\eta}(Y248)$	1.71 ± 0.12 (2.79 ± 0.16[b])	2.8[b]
$H_{\eta}(Y2')\cdots O_{\delta 2}(D256)$	1.63 ± 0.16 (2.72 ± 0.20[b])	3.5[b]
$H_{12}(R145)\cdots O_{\tau 1}(Y2')$	1.73 ± 0.15 (2.89 ± 0.18[a])	3.3[a]
$H_{22}(R145)\cdots O_{\tau 1}(Y2')$	1.69 ± 0.19 (2.73 ± 0.24[a])	3.0[a]

[a] Distance of N−O. [b] Distance of O−O.

the backbone root-mean-square deviation (rmsd) of 0.87 ± 0.04 Å, as shown in Figure 3. A snapshot from the MD simulation is displayed in Figure 4, and several statistically averaged geometric parameters are listed in Table 1. For comparison, the corresponding high-resolution crystallographic data are also included in the table. Our MD simulation indicated that the coordination sphere of the zinc ion is well-maintained. This is evidenced by the distances between the metal ion and three protein ligands, 1.99 ± 0.04 Å for $d_{Zn\cdots N_{\delta}(H69)}$, 2.13 ± 0.03 Å for $d_{Zn\cdots O_{\varepsilon}(E72)}$, and 2.00 ± 0.06 Å for $d_{Zn\cdots N_{\delta}(H196)}$. Meanwhile, the zinc ion is chelated by substrate carbonyl oxygen (O) and terminal amino nitrogen (N) atoms of G1′, with 2.39 ± 0.18 Å for $d_{Zn\cdots O(G1')}$ and 2.13 ± 0.11 Å for $d_{Zn\cdots N(G1')}$. These calculated distances are in fairly good agreement with the X-ray structure.[13]

The C-terminal of the substrate is further stabilized by various hydrogen bonds with protein residues. The carboxylate group of the Tyr residue (Y2′) forms a salt bridge with the side chain of Arg145, with the corresponding $H_{12}(R145)\cdots O_{\tau 1}(Y2')$ and $H_{22}(R145)\cdots O_{\tau 2}(Y2')$ distances of 1.73 ± 0.15 and 1.69 ± 0.19 Å, respectively. It forms a hydrogen bond with Tyr248 as well. The backbone amide N of Y2′ is hydrogen-bonded with the carboxylate group of the Glu270, with the $HN(Y2')\cdots O_{\varepsilon 1}$-(E270) distance of 2.01 ± 0.27 Å, while the phenolic group of the Y2′ is hydrogen-bonded with Asp256. As shown in Table 1,

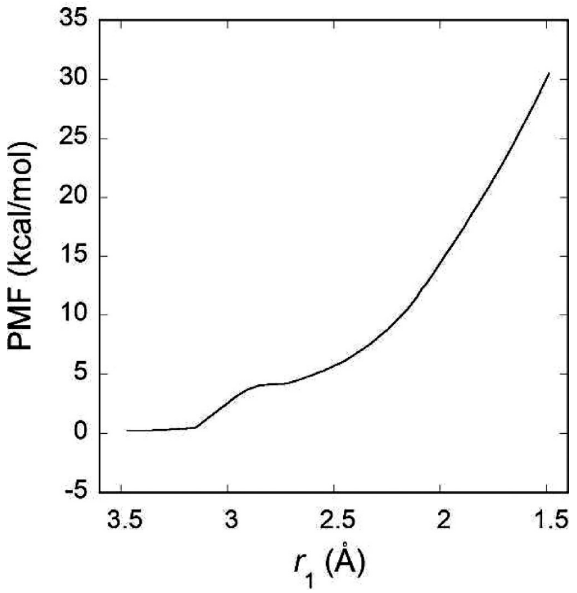

Figure 5. Free-energy profile for the acylation (A) step in the neutral model.

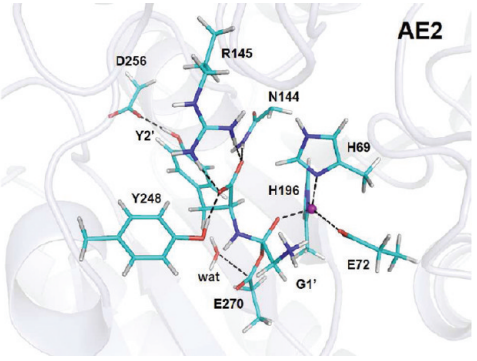

Figure 6. Snapshot from the MD simulation of the AE intermediate (AE2) of the nucleophilic pathway in the ionic model.

however, the former seems to overestimates, while the latter underestimates. Additionally, another hydrogen bond formed between Ser199 and Glu270 with $d_{H_{\gamma}(S199)\cdots O_{\varepsilon}(E270)} = 1.66 \pm 0.15$ Å. Ser197 also forms a hydrogen bond with the amino group of G1′ with the $O(S197)\cdots H_{\tau 1}(G1')$ distance of 1.76 ± 0.19 Å.

dx.doi.org/10.1021/jp2046504 |J. Phys. Chem. B 2011, 115, 10360–10367

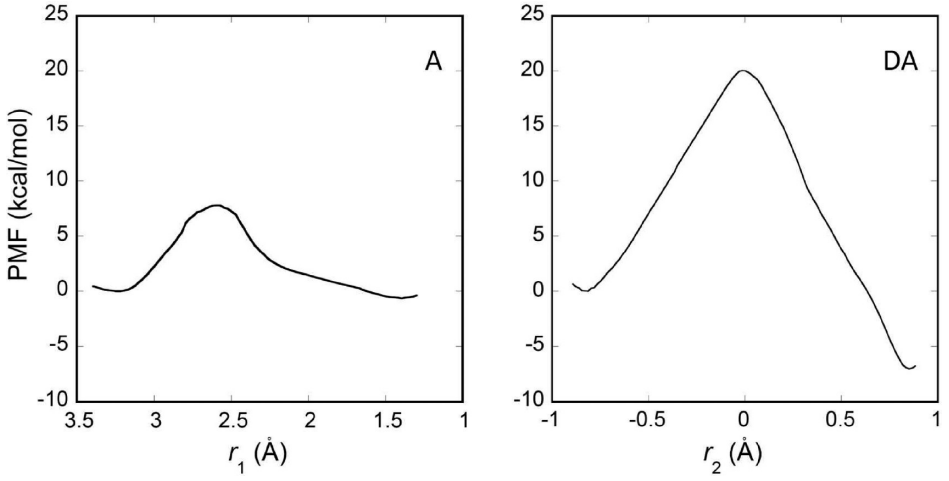

Figure 7. Free-energy profiles for the acylation (A) and deacylation (DA) steps in the ionic model. AE1 and AE2 differ in that AE2 includes the nucleophilic water in the QM region.

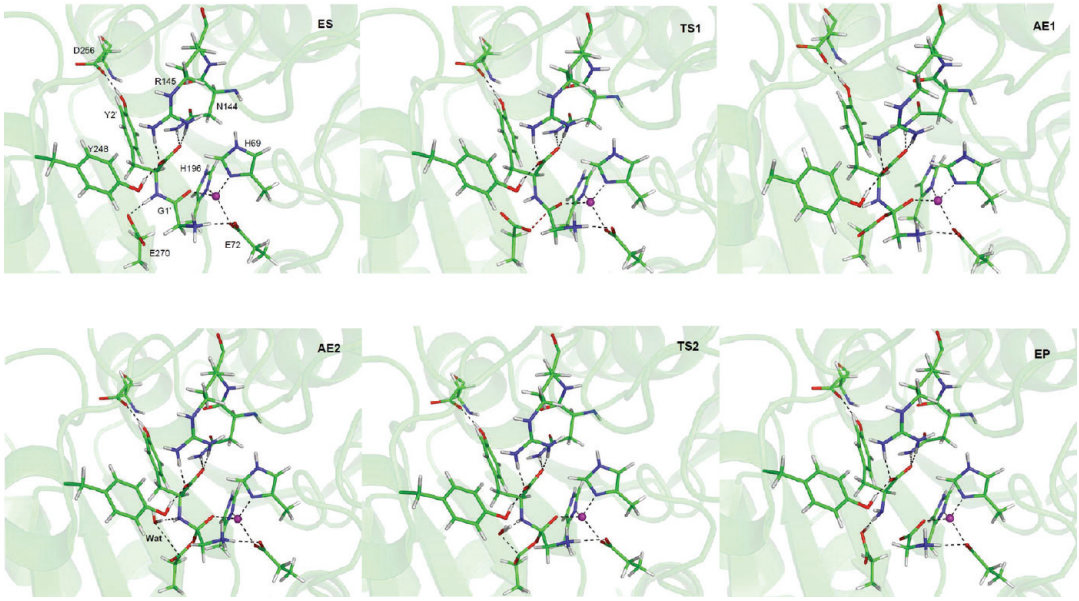

Figure 8. Stationary state structures for the ionic model via the nucleophilic mechanism.

The calculated geometric parameters are in reasonably good agreement with the well-resolved X-ray structure by Christianson and Lipscomb,[13] further validating the model.

As recognized before, the binding mode of GY is not optimal for hydrolysis. First of all, the chelation of the zinc ion clearly excludes the water nucleophile from binding with the metal ion, thus making the promoted water pathway infeasible. On the other hand, the active site is not in a good near-attack configuration either for nucleophilic addition of Glu270. For instance, the distance between the nucleophile (Glu270) and the scissile carbonyl carbon is far; the distance of $C(G1')\cdots O_{\varepsilon 2}(E270)$ is 4.88 ± 0.29 Å. As shown in Table 1, this distance is significantly larger than that observed in the X-ray structure (3.6 Å). In addition, the $O_{\varepsilon 2}(E270)\cdots C(G1')\cdots O(G1')$ angle of ~170° is from the optimal perpendicular nucleophilic attacking direction.

To test its reactivity, we have computed the PMF for the A step within the nucleophilic pathway along the putative reaction coordinate r_1. As shown in Figure 5, the free-energy profile increases monotonically, and no minimum could be located for the AE intermediate. This nonproductive free-energy curve probably stems partially with the unfavorable alignment of the reactant species discussed above. Perhaps more importantly, however, it might be attributed to the fact that the carbonyl oxygen of the scissile bond is quite far (2.39 ± 0.18 Å) away from the zinc ion and thus unable to provide stabilization for the AE complex. The fact that the GY is nonreactive with the neutral N-terminal amino group is consistent with the observation that this dipeptide is a competitive inhibitor in a basic environment.[39]

3.2. Ionic Model. The protonation of the N-terminal amino group in GY significantly altered its binding pattern. Although the rmsd of the MD simulation is still low, 0.85 ± 0.03 Å as shown in Figure 3, there are some significant differences between the two models. For example, the zinc ion is now tetracoordinated by substrate carbonyl oxygen with a $Zn\cdots O(G1')$ distance of

2.18 ± 0.11 Å while maintaining its coordination with the side-chain groups of protein His69, Glu72, and His196. On the other hand, the N-terminal ammonium group of the substrate forms a hydrogen bond with the carboxylate group of Glu72.

There is no X-ray structure of the CPA−GY complex that resembles ES_{ionic} observed in our simulation. Hence, there is no direct evidence in support of the mode of binding depicted here. However, we believe that the CPA binding pocket for the C-terminal residue is sufficiently specific to force the ligand in a similar pose as in $ES_{neutral}$, which was observed experimentally.[13] Indeed, the C-terminal carboxylate group of the Y2′ of the substrate forms a salt bridge with the side chain of the Arg145, and the corresponding hydrogen bond distances are $d_{H_{1\delta}(R145)\cdots O_{\tau}(Y2')} = 1.78 \pm 0.16$ Å and $d_{H_{1\delta}(R145)\cdots O_{\tau}(Y2')} = 1.78 \pm 0.16$ Å, respectively. This group is hydrogen-bonded with Asn144 and Tyr248 as well. The backbone amide NH group of the Y2′ is found to be hydrogen-bonded with the side-chain group of the Glu270, with a distance of 2.19 ± 0.27 Å for $HN(Y2')\cdots O_{\varepsilon 1}(E270)$. In addition, the side-chain phenolic group of the Tyr2′ is further stabilized by Glu256. These interactions resemble those in $ES_{neutral}$.

To consider the possible promoted water mechanism, we have simulated the ES_{ionic} complex with a water molecular ligated with the zinc ion. As discussed in the SI, our MD simulation for this model found that the water molecule was quickly expelled from the active site and the original binding pattern of ES_{ionic} was recovered. This observation suggests that the active site water cannot compete with the ionic form of the GY substrate in binding. As a result, we will only consider the nucleophilic pathway below.

The coordination of the scissile carbonyl group to the zinc ion observed in the ES_{ionic} complex suggests that the substrate might be amenable to the nucleophilic attack by Glu127. Indeed, the free-energy profile in Figure 6 for the nucleophilic addition indicates the formation of an AE complex. The free-energy barrier for the A step is 7.8 kcal/mol, and the reverse barrier is 8.5 kcal/mol. This indicates that the AE intermediate is reasonably stable and can be trapped at low temperatures. Our results thus provide support for the low-temperature solid-state NMR experiment by Lee et al., where an anhydride intermediate was detected in the CPA-catalyzed hydrolysis of GY.[41]

To obtain more details of the AE complex, we carried out a 700 ps MD simulation. The covalent acyl−enzyme bond is quite stable throughout the simulation, as evidenced by the distance of $d_{C(G1')\cdots O_{\varepsilon 1}(E270)} = 1.42 \pm 0.11$ Å. As described above, an additional water molecule was added to the QM region. The water molecule, which serves as the nucleophile in the following DA step, was found between the substrate and Glu270 during the MD simulation. The corresponding hydrogen bond distance is

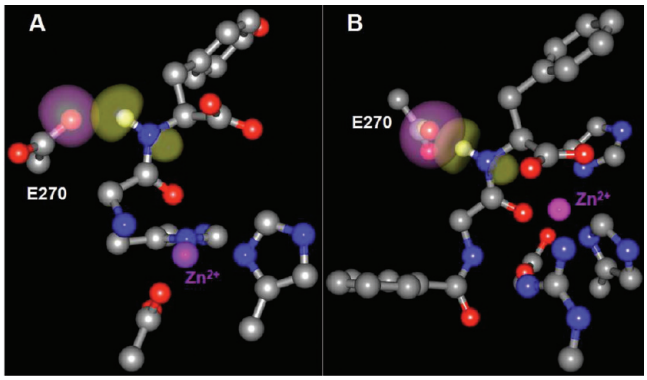

Figure 9. Natural orbitals for the hydrogen bond between the nucleophilic carboxylate of Glu270 and GY (A) or HPA (B).

Table 2. Selected Geometric Parameters of Stationary Points for the Ionic Model Obtained at the SCC-DFTB/MM Level of Theory[a]

	QM/MM							
distance (Å)	ES	TS1	AE1	AE2	TS2	EP	MD ES	MD AE2
$H_1\cdots O_w$				0.97	1.42	1.98		1.00 ± 0.02
$H_1\cdots N(Y2')$				2.01	1.13	1.02		1.99 ± 0.18
$O_w\cdots C_{\delta}(E270)$				3.01	1.96	1.38		3.01 ± 0.23
$C_{\delta}(E270)\cdots O_{\varepsilon 2}(E270)$				1.37	1.49	2.62		1.38 ± 0.06
$C(G1')\cdots O_{\varepsilon 2}(E270)$	3.47	2.02	1.43	1.43	1.48	3.47	3.41 ± 0.26	1.41 ± 0.08
$C(G1')\cdots N(Y2')$	1.33	1.37	1.45	1.48	1.55	2.65		1.49 ± 0.03
$C(G1')\cdots O(G1')$	1.27	1.28	1.38	1.38	1.36	1.30		1.36 ± 0.04
$C(G1')\cdots C_{\alpha}(G1')$	1.51	1.52	1.56	1.57	1.55	1.54		1.57 ± 0.06
$HN(Y2')\cdots O_{\varepsilon 1}(E270)$	1.82	3.16	2.17	2.19	3.08	4.04	2.19 ± 0.27	2.27 ± 0.31
$Zn\cdots N_{\delta 1}(H69)$	1.97	2.00	2.01	2.01	2.00	1.99	2.02 ± 0.03	2.02 ± 0.06
$Zn\cdots O_{\varepsilon 2}(E72)$	2.11	2.13	2.16	2.17	2.15	2.13	2.16 ± 0.05	2.16 ± 0.02
$Zn\cdots N_{\delta 1}(H196)$	1.96	1.97	1.99	1.99	1.98	1.97	1.99 ± 0.08	1.98 ± 0.04
$Zn\cdots O(G1')$	2.15	2.10	2.01	2.04	2.07	2.04	2.18 ± 0.11	2.08 ± 0.03
$O_{\tau 1}(Y2')\cdots H_{21}(N144)$	1.87	1.85	1.83	1.89	1.88	1.85	1.85 ± 0.28	1.86 ± 0.25
$O_{\tau 2}(Y2')\cdots H_{\eta}(Y248)$	1.57	1.56	1.56	1.55	1.55	1.57	1.64 ± 0.13	1.56 ± 0.16
$H_{\eta}(Y2')\cdots O_{\delta 2}(D256)$	1.54	1.55	1.54	1.54	1.54	1.55	1.68 ± 0.16	1.58 ± 0.18
$H_{12}(R145)\cdots O_{\tau 1}(Y2')$	1.81	1.81	1.79	1.78	1.79	1.85	1.78 ± 0.16	1.79 ± 0.19
$H_{22}(R145)\cdots O_{\tau 2}(Y2')$	1.63	1.61	1.60	1.61	1.64	1.58	1.71 ± 0.15	1.69 ± 0.13
$H_{\tau 3}(G1')\cdots O_{\varepsilon 2}(E72)$	1.78	1.80	1.79	1.82	1.79	1.83	1.83 ± 0.19	1.81 ± 0.16

[a] The statistically averaged geometries of the ES and AE2 complexes were taken from the MD simulation for the ionic model.

dx.doi.org/10.1021/jp2046504 |J. Phys. Chem. B 2011, 115, 10360–10367

Table 3. NBO Results for the N···HN···$O_{\varepsilon 1}$(E270) Hydrogen Bond in Three Different ES Complexes

ES complexes	bond length (Å)	bond angle (deg)	delocalized energy ΔE_2 (kcal/mol)	charge for $O_{\varepsilon 2}$(E270)
HPA−CPA	1.68	159.7	10.59	−0.738
GY−CPA	1.82	143.4	3.84	−0.811
HPL−CPA				−0.836

$d_{H_1\cdots O_{\varepsilon 1}(E270)}$ = 1.79 ± 0.25 Å. One of snapshots for the AE complex is demonstrated in Figure 7. The distance of $O_w\cdots C_\delta$-(E270) is 3.41 ± 0.26 Å in MD simulations, which suggests that the water is ready to attack at the C_δ position of E270. On the other hand, the ligand bond formed between the carbonyl oxygen and zinc ion (2.08 ± 0.03 Å) is also well-maintained throughout the MD simulation, which could provide additional stabilization of the AE intermediate.

The DA is initiated by the attack of the water nucleophile to the Glu270 carboxylate group, as indicated in Figure 1. (We have also tested the reaction path of a direct attack of water at the peptide carbonyl carbon, which clearly shows the monotonic increase of energy, and this path is thus nonproductive.) The DA step has a free-energy barrier of 20.1 kcal/mol, as shown in Figure 6. The barrier of this rate-determining step is in excellent agreement with the experimental value of 19.9 kcal/mol (estimated from the k_{cat} = 0.9 min^{-1}).[40] The stationary states along the reaction coordinates for both A and DA steps are displayed in Figure 8, and selected geometrical parameters are listed in Table 1.

3.3. Differences between GY and HPA. There are some interesting differences between the dipeptide (GY) and the peptide model used in our earlier work (HPA).[31] The latter was shown to be unreactive for the nucleophilic mechanism. A key reason, as we mentioned in our previous work,[31,32] is the hydrogen between the backbone amide and the side chain of Glu270, which weakens the nucleophilicity of the carboxylate group. This hydrogen bond is absent for the ester substrate (HPL), which becomes reactive.

To understand the role played by the hydrogen bond, we have carried out NBO studies on the truncated active site model for both CPA−GY and CPA−HPA complexes. The hydrogen bond energies extracted from our NBO calculations are listed in Table 3, and corresponding calculated NBO orbitals are displayed in Figure 9. Our results indicate that the hydrogen bond in the HPA−CPA complex is considerably stronger than that in the GY−CPA complex. The corresponding calculated delocalized energy ΔE_2 of the former is 10.59 kcal/mol, which is 6.75 kcal/mol higher than that of the latter. In the mean time, the charge on the nucleophilic oxygen is substantially higher in the CPA−GY complex. The weak hydrogen bond in the GY−CPA is presumably responsible for its reactivity. Indeed, this hydrogen bond is broken during the nucleophilic attack of the scissile carbonyl carbon; see Table 2.

The differences in the aforementioned hydrogen bond strength stem from the structures of the two ES complexes. The bulkier hippuryl group in HPA makes the backbone much more rigid than that in GY. In addition, the HPA substrate is hydrogen-bonded with the side chain of Arg127 and further rigidifies the backbone. This hydrogen bond is not observed in the CPA−GY complex.

4. CONCLUSIONS

In this work, we reported a computational study for the binding and the reactivity of a slowly hydrolyzing substrate, GY, in the active site of CPA. Our hybrid QM/MM simulations reproduced the X-ray structure of the GY−CPA complex when the substrate N-terminal amide group was in a neutral form. However, this represents a nonproductive binding configuration as the zinc is chelated by the substrate, in agreement with the experimental findings that the dipeptide is an inhibitor of CPA at high pH.

Our simulations further show that the proteolysis of the GY substrate is only viable for the ionic form of its N-terminal amide group. The nucleophilic pathway depicts the addition of the carboxylate group of Glu270 to the scissile carbonyl carbon, leading to a relatively stable AE complex. This observation is consistent with the low-temperature NMR experiment of Lee et al., who observed the anhydride intermediate. The DA step was found to be the rate-limiting step, with a free-energy barrier of 20.1 kcal/mol. This high barrier is consistent with the slowness of the reaction (k_{cat} = 0.9 min^{-1}).

The pH-dependent reactivity of the dipeptide discussed here might have important implications for drug design. For example, by making the amino group more basic, it is possible to design analogues of he dipeptide to serve as inhibitors of CPA. Indeed, this has been demonstrated by Lee and Kim,[42] who showed that *N*-(hydroxyacetyl)-L-phenylalaine is a strong inhibitor of CPA. This designing principle might be applicable in other zinc hydrolases.

■ ASSOCIATED CONTENT

Supporting Information. Comparison of SCC-DFTB/MM and B3LYP/MM reaction profiles and the MD simulations of the CPA complexed with the ionic form of GY and a water. This material is available free of charge via the Internet at http://pubs.acs.org.

■ AUTHOR INFORMATION

Corresponding Author

*E-mail: dgxu@scu.edu.cn.

Author Contributions

⊥Both authors contributed equally to this work.

■ ACKNOWLEDGMENT

This work was funded by the Natural Science Foundation of China (20803048 and 21073125) and by the Program for New Century Excellent Talents in University (NCET-10-0606) to D.X. and by the National Institutes of Health (R03-AI071992) to H.G. The authors are grateful to Prof. Qiang Cui for sharing with us the SCC-DFTB/CHARMM interface codes and for many useful discussions.

■ REFERENCES

(1) Vallee, B. L.; Galdes, A.; Auld, D. S.; Riordan, J. F. In *Zinc Enzymes*; Spiro, T. G., Ed. 1983.
(2) Lipscomb, W. M.; Strater, N. *Chem. Rev.* **1996**, *96*, 2375–2433.
(3) Ondetti, M. A.; Rubin, B.; Cushman, D. W. *Science* **1977**, *196* 441–444.
(4) Cushman, D. W.; Ondetti, M. A. *Nat. Med.* **1999**, *5*, 1110–1113.

(5) Christianson, D. W.; Lipscomb, W. N. *Acc. Chem. Res.* **1989**, *22*, 62–69.
(6) Rees, D. C.; Lipscomb, W. N. *J. Mol. Biol.* **1982**, *160*, 475–498.
(7) Rees, D. C.; Lipscomb, W. N. *Proc. Natl. Acad. Sci. U.S.A.* **1983**, *80*, 7151–7154.
(8) Rees, D. C.; Lipscomb, W. N. *J. Mol. Biol.* **1983**, *168*, 367–387.
(9) Christianson, D. W.; Lipscomb, W. N. *Proc. Natl. Acad. Sci. U.S.A.* **1985**, *82*, 6840–6844.
(10) Christianson, D. W.; Kuo, L. C.; Lipscomb, W. N. *J. Am. Chem. Soc.* **1985**, *107*, 8281–8283.
(11) Christianson, D. W.; Lipscomb, W. N. *J. Am. Chem. Soc.* **1986**, *108*, 545–546.
(12) Christianson, D. W.; Lipscomb, W. N. *J. Am. Chem. Soc.* **1986**, *108*, 4998–5003.
(13) Christianson, D. W.; Lipscomb, W. N. *Proc. Natl. Acad. Sci. U.S. A.* **1986**, *83*, 7568–7572.
(14) Christianson, D. W.; Lipscomb, W. N. *J. Am. Chem. Soc.* **1987**, *109*, 5536–5538.
(15) Christianson, D. W.; Lipscomb, W. N. *J. Am. Chem. Soc.* **1988**, *110*, 5560–5565.
(16) Kim, H.; Lipscomb, W. N. *Biochemistry* **1990**, *29*, 5546–5555.
(17) Mangani, S.; Carloni, P.; Orioli, P. *J. Mol. Biol.* **1992**, *223* 573–578.
(18) Teplyakov, A.; Wilson, K. S. *Acta Crystallogr.* **1993**, *D49* 534–540.
(19) Greenblatt, H. M.; Feinberg, H.; Tucker, P. A.; Shoham, G. *Acta Crystallogr.* **1998**, *D54*, 289–305.
(20) Cho, J. H.; Kim, D. H.; Chung, S. J.; Ha, N.-C.; Oh, B.-H.; Choi, K. Y. *Bioorg. Med. Chem.* **2002**, *10*, 2015–2022.
(21) Kilshtain-Vardi, A.; Glick, M.; Greenblatt, H. M.; Goldblum, A.; Shoham, G. *Acta Crystallogr.* **2003**, *D59*, 323–333.
(22) Breslow, R.; Wernick, D. L. *J. Am. Chem. Soc.* **1976**, *98* 259–261.
(23) Breslow, R.; Wernick, D. L. *Proc. Nat. Acad. Sci. U.S.A.* **1977**, *74* 1303–1307.
(24) Auld, D. S.; Galdes, A.; Geoghegan, K. F.; Holmquit, B.; Martinelli, R. A.; Vallee, B. L. *Proc. Natl. Acad. Sci. U.S.A.* **1984**, *81* 5041–5045.
(25) Geoghegan, K. F.; Galdes, A.; Hanson, G.; Holmquit, B.; Auld, D. S.; Vallee, B. L. *Biochemistry* **1986**, *25*, 4669–4674.
(26) Makinen, M. W.; Kuo, L. C.; Dymowski, J. J.; Jaffer, S. *J. Biol. Chem.* **1979**, *254*, 356–366.
(27) Kuo, L. C.; Makinen, M. W. *J. Biol. Chem.* **1982**, *257*, 24–27.
(28) Suh, J.; Cho, W.; Chung, S. *J. Am. Chem. Soc.* **1985**, *107* 4530–4535.
(29) Sander, M. E.; Witzel, H. *Biochem. Biophys. Res. Commun.* **1985**, *132*, 681.
(30) Britt, B. M.; Peticolas, W. L. *J. Am. Chem. Soc.* **1992**, *114* 5295–5303.
(31) Xu, D.; Guo, H. *J. Am. Chem. Soc.* **2009**, *131*, 9780–9788.
(32) Wu, S.; Zhang, C.; Xu, D.; Guo, H. *J. Phys. Chem. B* **2010**, *114*, 9259–9267.
(33) Alvarez-Santos, S.; Gonzalez-Lafont, A.; Lluch, J. M.; Oliva, B.; Aviles, F. X. *New J. Chem.* **1998**, 319–325.
(34) Vardi-Kilshtain, A.; Shoham, G.; Goldblum, A. *Mol. Phys.* **2003**, *101*, 2715–2724.
(35) Cross, J. B.; Vreven, T.; Meroueh, S. O.; Mobashery, S.; Schlegel, H. B. *J. Phys. Chem. B* **2005**, *109*, 4761–4769.
(36) Szeto, M. W. Y.; Mujika, J. I.; Zurek, J.; Mulholland, A. J.; Harvey, J. N. *J. Mole. Struct.: THEOCHEM* **2009**, *898*, 106–114.
(37) Vardi-Kilshtain, A.; Warshel, A. *Proteins* **2009**, *77*, 536–550.
(38) Yanari, S.; Mitz, M. A. *J. Am. Chem. Soc.* **1956**, *79*, 1150–1153.
(39) Yanari, S.; Mitz, M. A. *J. Am. Chem. Soc.* **1956**, *79*, 1154–1158.
(40) Izumiya, N.; Uchio, H. *J. Biochem.* **1959**, *46*, 235–245.
(41) Lee, H. C.; Ko, Y. H.; Baek, S. B.; Kim, D. H. *Bioorg. Med. Chem. Lett.* **1998**, *8*, 3379–3384.
(42) Lee, K. J.; Kim, D. H. *Bioorg. Med. Chem.* **1998**, *6*, 1613–1622.
(43) Warshel, A.; Levitt, M. *J. Mol. Biol.* **1976**, *103*, 227–249.
(44) Gao, J.; Ma, S.; Major, D. T.; Nam, K.; Pu, J.; Truhlar, D. *Chem. Rev.* **2006**, *106*, 3188–3209.
(45) Riccardi, D.; Schaefer, P.; Yang, Y.; Yu, H.; Ghosh, N.; Prat-Resina, X.; Konig, P.; Li, G.; Xu, D.; Guo, H.; Elstener, M.; Cui, Q. *J. Phys. Chem. B* **2006**, *110*, 6458–6469.
(46) Senn, H. M.; Thiel, W. *Angew. Chem., Int. Ed.* **2009**, *48*, 1198–1229.
(47) Gao, J. In *Rev. Comput. Chem.*; Lipkowitz, K. B., Boyd, D. B., Eds.; VCH: New York, 1996; Vol. 7, pp 119−185.
(48) Elstner, M.; Porezag, D.; Jungnickel, G.; Elsner, J.; Haugk, M.; Frauenheim, T.; Suhai, S.; Seigert, G. *Phys. Rev.* **1998**, *B58*, 7260–7268.
(49) MacKerell, A. D., Jr.; Bashford, D.; Bellott, M.; Dunbrack, R. L., Jr.; Evanseck, J. D.; Field, M. J.; Fischer, S.; Gao, J.; Guo, H.; Ha, S.; Joseph-McCarthy, D.; Kuchnir, L.; Kuczera, K.; Lau, F. T. K.; Mattos, C.; Michnick, S.; Ngo, T.; Nguyen, D. T.; Prodhom, B.; Reiher, W. E., III; Roux, B.; Schlenkrich, M.; Smith, J. C.; Stote, R.; Straub, J.; Watanabe, M.; Wiorkiewicz-Kuczera, J.; Yin, D.; Karplus, M. *J. Phys. Chem. B* **1998**, *102*, 3586–3616.
(50) Cui, Q.; Elstner, M.; Kaxiras, E.; Frauenheim, T.; Karplus, M. *J. Phys. Chem. B* **2001**, *105*, 569–585.
(51) Elstner, M.; Cui, Q.; Munih, P.; Kaxiras, E.; Frauenheim, T.; Karplus, M. *J. Comput. Chem.* **2003**, *24*, 565–581.
(52) Xu, D.; Zhou, Y.; Xie, D.; Guo, H. *J. Med. Chem.* **2005**, *48* 6679–6689.
(53) Xu, D.; Xie, D.; Guo, H. *J. Biol. Chem.* **2006**, *281*, 8740–8747.
(54) Wang, C.; Guo, H. *J. Phys. Chem. B* **2007**, *111*, 9986–9992.
(55) Xu, D.; Guo, H.; Cui, Q. *J. Phys. Chem. A* **2007**, *111*, 5630–5636.
(56) Xu, D.; Guo, H.; Cui, Q. *J. Am. Chem. Soc.* **2007**, *129*, 10814.
(57) Wu, S.; Xu, D.; Guo, H. *J. Am. Chem. Soc.* **2010**, *132* 17986–17988.
(58) Jorgensen, W. L.; Chandrasekhar, J.; Madura, J. D.; Impey, R. W.; Klein, M. L. *J. Chem. Phys.* **1983**, *79*, 926–935.
(59) Brooks, C. L., III; Brunger, A.; Karplus, M. *Biopoly.* **1985**, *24*, 843.
(60) Field, M. J.; Bash, P. A.; Karplus, M. *J. Comput. Chem.* **1990**, *11* 700–733.
(61) Steinbach, P. J.; Brooks, B. R. *J. Comput. Chem.* **1994**, *15*, 667.
(62) Ryckaert, J. P.; Ciccotti, G.; Berendsen, H. J. *J. Comput. Phys.* **1977**, *23*, 327–341.
(63) Guest, M. F.; Bush, I. J.; van Dam, H. J. J.; Sherwood, P.; Thomas, J. M. H.; van Lenthe, J. H.; Havenith, R. W. A.; Kendrick, J. *Mol. Phys.* **2005**, *103*, 719.
(64) Torrie, G. M.; Valleau, J. P. *J. Comput. Phys.* **1977**, *23*, 187–199.
(65) Kumar, S.; Bouzida, D.; Swendsen, R. H.; Kollman, P. A.; Rosenberg, J. M. *J. Comput. Chem.* **1992**, *13*, 1011–1021.
(66) Weinhold, F.; Landis, C. R. *Valency and Bonding. A Natural Bond Orbital Donor-Acceptor Perspective*; Cambridge University Press: Cambridge, U.K., 2005.